Black and gray Helmholtz-Kerr soliton refraction

Julio Sánchez-Curto* and Pedro Chamorro-Posada
Departamento de Teoría de la Señal y Comunicaciones e Ingeniería Telemática, Universidad de Valladolid, ETSI Telecomunicación, Paseo Belén 15, Valladolid ES-47011, Spain

Graham S. McDonald
Joule Physics Laboratory, School of Computing, Science and Engineering, Materials and Physics Research Centre, University of Salford, Salford M5 4WT, United Kingdom

(Received 17 September 2010; published 31 January 2011)

Refraction of black and gray solitons at boundaries separating different defocusing Kerr media is analyzed within a Helmholtz framework. A universal nonlinear Snell's law is derived that describes gray soliton refraction, in addition to capturing the behavior of bright and black Kerr solitons at interfaces. Key regimes, defined by beam and interface characteristics, are identified, and predictions are verified by full numerical simulations. The existence of a unique total nonrefraction angle for gray solitons is reported; both internal and external refraction at a single interface is shown possible (dependent only on incidence angle). This, in turn, leads to the proposal of positive or negative lensing operations on soliton arrays at planar boundaries.

DOI: 10.1103/PhysRevA.83.013828 PACS number(s): 42.65.Tg, 42.25.Gy

I. INTRODUCTION

Nonlinear interfaces constitute one of the most appealing fundamental research topics in nonlinear optics. Two reasons contribute substantially to interest. First, nonlinear interfaces exhibit a good number of nonlinear wave phenomena, such as the excitation of nonlinear surface waves (NSW) or soliton breakup. Second, nonlinear interfaces are a core element in proposed all-optical devices, such as optical switches or all-optical gates. The late 1970s and early 1980s witnessed pioneering works on nonlinear interfaces [1–7]. Nonlinear surface waves were first described in 1980 [4] when a linear–Kerr-type nonlinear interface was found to accommodate localized solutions that preserve their shape while traveling along the planar boundary. They have since been reported in contexts involving a great variety of media, such as linear–diffusing Kerr-type [8,9], two Kerr-type [10–13], saturable [14], and defocusing thermal media [15]. The stability [16] and excitation [9,17] of NSWs have been commonly studied in both single interface and nonlinear waveguide contexts. Soliton breakup at nonlinear interfaces was predicted in the numeric simulations of Rozanov [3]. In studying linear–Kerr-type interfaces, he described how the field entering the second medium is perturbed by the interface, and subsequently breaks up into multiple solitonlike beams. Several investigations revisited this effect for the same type of interfaces [7,18,19] as well as for those involving two focusing Kerr-type media [12]. Multisoliton bound states [19] and vector solitons [20] have also been found to break up at interfaces, whereby their fundamental components evolve independently as single solitonlike beams. Of particular interest has been the giant Goos-Hänchen shift (GHS). This is an enhanced version of the GHS at the planar boundary separating two linear dielectric media [21,22] when, instead, different types of nonlinear interfaces [5,7,12,19,23] are considered.

To detail potential applications of nonlinear interfaces in designs of all-optical devices, one must consider nonlinear waveguides. These structures were a focus of attention during the 1980s, and the discovery of many interface properties originated from the study of such waveguides. A range of both linear and nonlinear materials were proposed as waveguide layers, leading to a great variety of configurations [24–28]. The review of Mihalache *et al.* [29] summarizes early studies and proposes further applications, such as directional couplers [13,30,31]. Nonlinear interfaces have inherent switching behavior; combinations of high- and low-intensity beams can be used to modify angles of propagation, which, in turn, may switch a soliton from refraction to reflection at an interface. Linear-nonlinear interfaces with a diffusive Kerr-type medium [32], and interfaces separating two photorefractive media [33], have been proposed to support such switching behavior. All-optical gates, facilitated by the superposition of different Kerr-type materials, were also suggested [34–36]. In this case, a control soliton may modify interface properties, such that a signal soliton experiences either reflection or refraction, and constitutes a basis for design of AND and OR gates.

Experimental work on nonlinear interfaces has mostly been concerned with verification of theoretical predictions. The pioneering experiments of Smith *et al.* involved optical bistability [37] and the switching response of a linear-nonlinear interface [6,38]. It was later shown [39] that such interfaces tend to exhibit single-step, rather than multiple-threshold, response (particularly for saturable nonlinear media). The existence of critical angles at nonlinear interfaces was verified by Alvarado-Mendez *et al.* [40], where a nonlinear-linear interface (composed of a photorefractive crystal and air) was studied. Not only Kerr-type, but also quadratically nonlinear, media also have been analyzed [41,42], where it was shown that experimental results were in good agreement with those from full numerical integration of the coupled scalar wave equations for the fundamental and second harmonic fields. Recently, experiments on nonlinear interfaces have focused on nematicons [43–46], the reorientational dielectric response

*julsan@tel.uva.es

to an external voltage of which is the basis for inducing refractive index changes in a nonlinear material. Solitons undergoing tunable reflection or refraction [47], total internal reflection [47], nonspecular total reflection [48], or nonlinear Goos-Hänchen shifts along the planar boundary [49] have been engineered at nonlinear interfaces provided that adequate electric fields are applied. The ability of controlling soliton paths in a great variety of scenarios [50–52] turns them into excellent candidates to lie in the core of all-optical processing devices [53–56].

The successful particlelike approach developed by Aceves *et al.* [10–13] made a major impact on theoretical descriptions. A simple Newtonian model was found to capture complicated beam evolution at nonlinear interfaces. In this model, a soliton is represented by a quasiparticle that evolves in a potential defined by the interface. While initially describing Kerr interfaces, the theory was later developed to describe diffusive Kerr-type [8,57] and saturable Kerr [14] media. Further generalizations were made to analyze solitons at non-Kerr interfaces, such as those involving quadratic [58] and photorefractive [59] media. However, this equivalent-particle approach is based on the nonlinear Schrödinger (NLS) equation, for which the paraxial approximation is assumed and limits the validity of analysis to vanishingly small angles of incidence [60,61].

Soliton behavior at nonlinear interfaces has, instead, an inherently nonparaxial character that can arise in two distinct scenarios. First, significant off-axis nonparaxiality arises whenever a soliton is either incident or refracted at a significant angle to the interface. Even for low incidence angles, interfaces can result in a large angle of refraction. For example, a larger linear index of refraction in the second medium can produce this effect, and demand a theoretical framework able to accommodate arbitrary angles of propagation. Second, a completely different type of nonparaxiality can appear at nonlinear interfaces, which is related to strong focusing [62]. For example, if the strength of nonlinearity in the second medium is much larger than in the first medium, ultranarrow beams can originate from the interface. This would demand a vector analysis [63–65] to study properly the propagation of the emergent beams.

Our work deals only with the first type of angular (Helmholtz) nonparaxiality. Large angles of propagation are perfectly described within the framework of Helmholtz theory [66,67] where, unlike paraxial theory, solutions are rotationally invariant. The model equation is the full nonlinear Helmholtz (NLH) equation [62,66] without any further approximation. Not only bright Kerr, but also dark Kerr [68], two-component [69], boundary [70], bistable [71], and algebraic [72] Helmholtz solitons have been found to display nontrivial Helmholtz corrections. This latter framework has permitted, for instance, description of collisions of Kerr bright solitons at arbitrary angles [73]. The reflection and refraction properties of bright solitons [74,75] at the interface separating two focusing Kerr media have also been revisited within the framework of Helmholtz theory. A key result is a compact generalized Snell's law that relates soliton angles of incidence and refraction and that is valid for arbitrary angles.

Recently, the Helmholtz-Snell's law for bright solitons was generalized to describe black soliton refraction [76]. In contrast to the vast literature dealing with bright solitons at nonlinear interfaces, only a few works have considered interfaces separating defocusing media. Moreover, those studies were restricted to phenomena taking place in the vicinity of the interface. The formation of NSWs at interfaces, where at least one medium has a defocusing Kerr-type nonlinearity [77,78], or the generation of kink solitons at the surface of an optical lattice imprinted in defocusing media [79], represent two such examples. Unlike these works, developed within the framework of the NLS equation, Ref. [76] addresses for the first time the evolution of a dark soliton far away from the interface as the result of a refraction by a nonlinear interface separating two defocusing Kerr media. Black soliton refraction is fully characterized by the generalized Snell's law. A more in-depth analysis of gray soliton refraction was beyond the scope of Ref. [76] and is presented, instead, in this paper.

The nonlinear Snell's law is briefly revisited in Sec. II. This is the theoretical basis of our analysis. We then present a further generalized version that describes the refraction of not only black and bright solitons [74,76], but also of gray solitons. In Sec. III, consideration of the parameter defining the grayness of a dark soliton is shown to lead to refraction properties. Linear step interfaces (those with identical defocusing Kerr nonlinearities) are analyzed in Sec. IV. Section V introduces the total nonrefraction angle, which we prove is the unique angle of incidence for a gray soliton to be transmitted with an undeviated trajectory. It is shown to be an inherently nonparaxial quantity. We find that, in contrast to bright or black soliton refraction, gray solitons can undergo both internal and external refraction (dictated solely by the angle of incidence). This leads to a proposal of lensing properties of planar interfaces, which have potential in the manipulation of soliton arrays. Analytical expressions for nonrefraction angles are presented, and predicted behavior is verified by numerical simulations. Finally, a discussion of the numerical techniques employed is given in Sec. VI.

II. GENERALIZED SNELL'S LAW FOR GRAY SOLITONS

Analysis is based on the two-dimensional scalar Helmholtz equation

$$\frac{\partial^2 E}{\partial x^2}+\frac{\partial^2 E}{\partial z^2}+\frac{\omega^2}{c^2}n^2(x,z;|E|)E=0, \tag{1}$$

which describes propagation of a TE-polarized monochromatic optical beam in a nonlinear medium with refractive index $n(x,z;|E|)$. For the incidence and refraction Kerr media ($i=1$ and 2, respectively), considered in this work, $n=n_{0i}\pm\alpha_i|E|^2$, where $\alpha_i>0$ are the Kerr coefficients, and $\pm$ corresponds to either a focusing or a defocusing Kerr nonlinearity, respectively. The $E(x,z)$ is the time-independent complex field envelope of the optical beam with intensity $I=|E|^2$. When the longitudinal and transverse coordinates are scaled as $\zeta=z/L_D$ and $\xi=2^{1/2}x/w_0$, respectively, and one adopts a forward z-propagating phase reference $E(x,z)=A(x,z)e^{jkz}$, Eq. (1) can be rewritten as

$$\kappa\frac{\partial^2 A}{\partial\zeta^2}+j\frac{\partial A}{\partial\zeta}+\frac{1}{2}\frac{\partial^2 A}{\partial\xi^2}-\frac{1}{4\kappa}\left(1-\frac{n^2}{n_{01}^2}\right)A=0. \tag{2}$$

w_0 is a transverse scale parameter equal to the waist of a reference Gaussian beam with diffraction length $L_D=kw_0^2/2$,

$k = n_{01}\omega/c$ represents the wave number, and n_{01} is the linear refractive index of medium 1 (which we have used as a reference medium). In Eq. (2), $\kappa = 1/k^2 w_0^2$ is a nonparaxiality parameter [62,66] that relates the full width $2w_0$ of the reference beam to the optical wavelength in a vacuum. The only approximation made in this analysis is that, in each medium, $n_{0i} \ll \alpha_i |E|^2$. Under such conditions, one obtains $n^2 \approx n_{0i}^2 \pm 2n_{0i}\alpha_i |E|^2$.

For propagation in medium 2, which has $n = n_{02} \pm \alpha_2 |E|^2$, and using the normalization $A(\xi,\zeta) = ({n_{01}}^2/k\alpha_1 L_D n_{02})^{1/2} u(\xi,\zeta)$, Eq. (2) transforms to

$$\kappa \frac{\partial^2 u}{\partial \zeta^2} + j\frac{\partial u}{\partial \zeta} + \frac{1}{2}\frac{\partial^2 u}{\partial \xi^2} - \left(\frac{n_{01}^2 - n_{02}^2}{4\kappa n_{01}^2} \pm \frac{\alpha_2}{\alpha_1}|u|^2\right) u = 0. \tag{3}$$

The interface parameters, relating the linear and nonlinear refractive indices of the adjoining media,

$$\Delta \equiv 1 - \left(\frac{n_{02}}{n_{01}}\right)^2, \quad \alpha \equiv \frac{\alpha_2}{\alpha_1}, \tag{4}$$

allow us to rewrite Eqs. (2) and (3) in a compact form as

$$\kappa \frac{\partial^2 u}{\partial \zeta^2} + j\frac{\partial u}{\partial \zeta} + \frac{1}{2}\frac{\partial^2 u}{\partial \xi^2} \pm |u|^2 u = \left[\frac{\Delta}{4\kappa} \pm (1-\alpha)|u|^2\right] \chi(\xi,\zeta)\, u. \tag{5}$$

Here, $\chi(\xi,\zeta)$ identifies the two media separated by the planar boundary taking values 0 or 1 when (ξ,ζ) is in medium 1 or medium 2, respectively. In the particular case wherein the boundary is situated at $\xi = 0$, one has $\chi(\xi,\zeta) = H(\xi)$, i.e., the Heaviside function. The NLH equation (5) is fully equivalent to Eq. (1), since no further approximation has been made in its derivation.

Matching the phase of bright and black soliton solutions, for focusing [66,67,80] and defocusing [68] Kerr media, respectively, at each side of the discontinuity yields the nonlinear Snell's law [74–76]

$$\gamma_\pm n_{01} \cos(\theta_i) = n_{02} \cos(\theta_t), \tag{6}$$

which dictates refraction of both bright and black solitons. θ_i and θ_t are the angles of incidence and refraction, respectively, and

$$\gamma_\pm = \left[\frac{(1 + 4\kappa\beta_\pm)}{1 + 4\kappa\beta_\pm \alpha (1-\Delta)^{-1}}\right]^{1/2} \tag{7}$$

is a nonlinear correction term [76]. In Eq. (7), $\beta_+ = \eta_0^2/2$ and $\beta_- = -u_0^2$ for bright and black solitons, respectively, and η_0 and u_0 are the amplitudes of the incident bright soliton and the background plane wave supporting the black soliton, respectively.

Importantly, the refraction of gray solitons differs fundamentally from that associated with bright or black solitons. We find that the soliton grayness parameter significantly affects the net angle of propagation, which, in turn, alters the laws governing gray soliton refraction at nonlinear interfaces. Angular corrections in Eq. (6) are thus needed in order to capture such grayness dependency.

The Helmholtz dark soliton is [68,76]

$$u(\xi,\zeta) = u_0 (A \tanh\Theta + jF) \exp\left(\frac{-j\zeta}{2\kappa}\right) \times \exp\left[j\sqrt{\frac{1 - \Delta - 4\kappa u_0^2 \alpha}{1 + 2\kappa V^2}}\left(-V\xi + \frac{\zeta}{2\kappa}\right)\right], \tag{8}$$

where

$$\Theta = \frac{u_0 A \alpha^{1/2}(\xi + W\zeta)}{\sqrt{1 + 2\kappa W^2}} \quad \text{and} \quad W = \frac{V - V_0}{1 + 2\kappa V V_0}. \tag{9}$$

Here, $\Delta = 0$ and $\alpha = 1$ correspond to the propagation in medium 1; W is the net transverse velocity; $V = (2\kappa)^{1/2}\tan(\theta)$ is the transverse velocity of the background beam associated with an arbitrary propagation angle θ relative to the reference z axis [66]; and

$$V_0 = \frac{u_0 F \alpha^{1/2}}{\left[1 - \Delta - (2 + F^2) 2\kappa u_0^2 \alpha\right]^{1/2}} \tag{10}$$

is the intrinsic transverse velocity of a gray soliton in medium 2. In Eq. (8), u_0 is the amplitude of the soliton background and $F = (1 - A^2)^{1/2}$ is the grayness parameter ($F = 0$ for black solitons and $0 < |F| < 1$ for gray solitons) [68].

During refraction, the value of F is conserved [76]. This condition arises from the continuity of the phase across the interface which, in turn, requires the total intrinsic phase jump of a Helmholtz gray soliton [68,76]

$$\Delta\phi = -2\tan^{-1}\left(\frac{F}{\sqrt{1 - F^2}}\right) \tag{11}$$

to be the same in both media. Black (gray) solitons impinging on a nonlinear interface are thus refracted as black (gray) solitons in the second medium.

Taking into account the relationship linking transverse velocities (in normalized units) and angles (in the unscaled laboratory frame) [66,67], one obtains from Eq. (9)

$$\theta_{ni} = \theta_i - \theta_{0i} \quad \text{and} \quad \theta_{nt} = \theta_t - \theta_{0t}, \tag{12}$$

which are the angular relationships describing, respectively, the incident and refracted soliton. In Eq. (12), the subscripts i and t refer to the incident and transmitted (refracted) gray solitons found at each side of the interface, while θ_n, θ, and θ_0 are the angles corresponding to W, V, and V_0, respectively. The θ_{0i} and θ_{0t} are the intrinsic angles of the gray solitons related to the incident and transmitted gray solitons, respectively.

The angular relationships in Eq. (12) are shown in Fig. 1 where the interface, represented by a solid white line, has been rotated in relation to the reference axes. The white arrow represents the propagation of the background plane wave, or the corresponding black soliton, incident on the interface at an angle θ_i and refracted at an angle θ_t. Under the same conditions, a gray soliton represented by a dashed line impinges on the interface at a net angle of $\theta_{ni} < \theta_i$ as a result of the intrinsic angle of the incident soliton θ_{0i}. The corresponding intrinsic component for the refracted soliton θ_{0t} makes the net angle of refraction of the gray soliton θ_{nt} differ from θ_t.

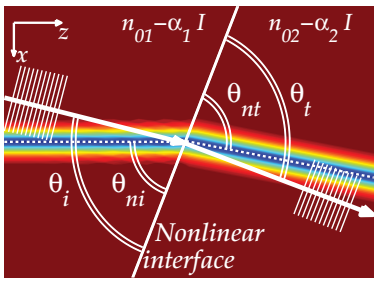

FIG. 1. (Color online) Angles of incidence and refraction for both black and gray solitons in relation to the nonlinear interface.

From the above arguments, Eq. (6) can now be rewritten as

$$\gamma_{\pm} n_{01} \cos(\theta_{ni} + \theta_{0i}) = n_{02} \cos(\theta_{nt} + \theta_{0t}). \tag{13}$$

Equation (13) is supplemented with the condition of conservation of soliton grayness during refraction, which allows one to obtain the value of θ_{0t} from that of θ_{0i}. We have thus derived a generalized Snell's law that is also valid for gray solitons. The law is expressed in terms of both net propagation angles and intrinsic angular components of the gray soliton dips. When $\theta_{0i} = \theta_{0t} = 0$, this generalized Snell's law (13) returns the previously reported results [74,76] for bright (γ_+) and black (γ_-) solitons.

Bright, black, and gray soliton refractions are illustrated in Fig. 2 for a nonlinear interface ($\Delta = -0.026$ and $\alpha = 3$) and two values of κ. Assuming canonical bright ($\eta_0 = 1$) and dark ($u_0 = 1$) solitons, two different scenarios are found, which are distinguished by the size of κ. For $\kappa = 10^{-4}$, one obtains $|\Delta| \gg 4\kappa u_0^2$ and $|\Delta| \gg 2\kappa\eta_0^2$, so that the soliton refraction characteristics are governed by Δ. This is demonstrated in Fig. 2(a), where all soliton types undergo external refraction with comparable angles of refraction. The scenario changes completely when $\kappa = 2.5 \times 10^{-3}$, as is shown in Fig. 2(b). Here, one has $|\Delta| \sim 4\kappa u_0^2$ and $|\Delta| \sim 2\kappa\eta_0^2$, so that nonlinear terms may induce different angular corrections in each case, thus leading to more distinct angles of refraction for each soliton type. While bright and black solitons undergo external refraction ($\theta_{nt} > \theta_{ni}$), the gray soliton experiences internal refraction ($\theta_{nt} < \theta_{ni}$).

Numerical evidence of the validity of Eq. (13) for describing bright [74,75] and black [76] soliton refraction has already been demonstrated. The qualitative behavior dictated by

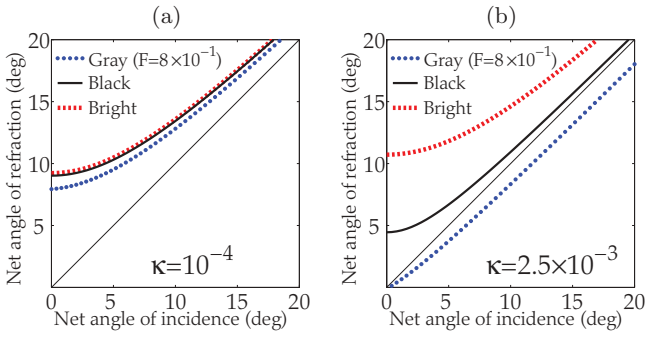

FIG. 2. (Color online) Generalized Snell's law for bright (dashed red), black (solid black), and gray (dotted blue) solitons. (a) $\kappa = 10^{-4}$ and (b) $\kappa = 2.5 \times 10^{-3}$.

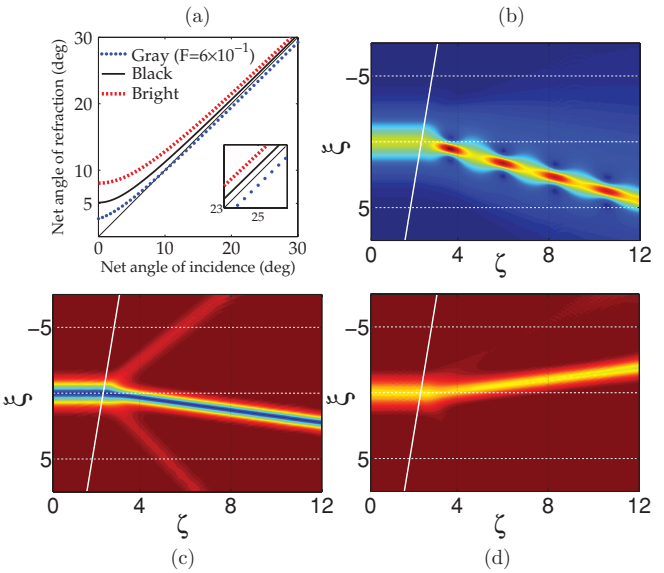

FIG. 3. (Color online) (a) Generalized Snell's law for bright, black, and gray solitons, when $\kappa = 10^{-3}$, $u_0 = 1$, and $\eta_0 = 1$. Full simulation of (b) bright, (c) black, and (d) gray soliton refractions when $\theta_{ni} = 25^{\circ}$.

Eq. (13) for bright, black, and gray soliton refraction is illustrated in Fig. 3. Theoretical results shown in Fig. 3(a) for $\alpha = 3$ and $\Delta = -0.016$, predicting either internal or external refraction, agree well with numerical simulations undertaken for Figs. 3(b) bright, 3(c) black, and 3(d) gray solitons impinging on the interface at $\theta_{ni} = 25^{\circ}$. As the inset of Fig. 3(a) shows, only the gray soliton undergoes internal refraction.

Even when additional solitons appear, Snell's law predicts accurately the refraction of the primary black or gray soliton. Conditions for multiple soliton generation during refraction of black solitons are the subject of a forthcoming paper, where both bright and black soliton breakup at nonlinear interfaces is studied within the framework of Helmholtz theory.

III. ROLE OF THE GRAYNESS PARAMETER

Analysis of gray soliton refraction clearly must focus on the role of the intrinsic angular terms associated with the soliton grayness parameter, i.e., θ_{0t} and θ_{0i}. For the sake of simplicity, we will assume that $F > 0$, so that both θ_{0t} and θ_{0i} are positive. Within the framework of Helmholtz theory, analysis of broad beams (when compared to the wavelength) of moderate intensity implies that $\kappa = 1/(kw_0)^2 \ll 1$ and $4\kappa u_0^2 \ll 1$. Then, considering a regime in which both linear and nonlinear terms are of the same order of magnitude, i.e., $\Delta \sim 4\kappa u_0^2$, one obtains from Eqs. (9) and (10)

$$\tan\theta_{0i} \sim \sqrt{2\kappa} F u_0 \left[1 + (2 + F^2)\kappa u_0^2\right] \tag{14}$$

and

$$\tan\theta_{0t} \sim \sqrt{2\kappa\alpha} F u_0 \left[1 + \frac{\Delta}{2} + \alpha(2 + F^2)\kappa u_0^2\right], \tag{15}$$

respectively. Equation (15) reveals that θ_{0t} depends strongly on $\alpha^{1/2}$. This is shown in Fig. 4(a), where the difference $\theta_{0t} - \theta_{0i}$ is plotted as a function of α for two values of F.

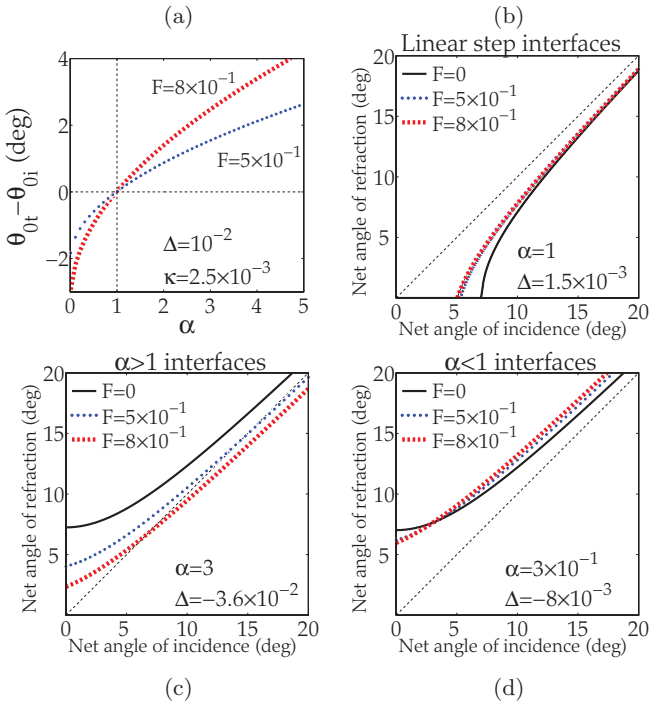

FIG. 4. (Color online) (a) The difference $\theta_{0t} - \theta_{0i}$ as a function of α. Generalized Snell's law for dark solitons at interfaces with (b) $\alpha = 1$, (c) $\alpha > 1$, and (d) $\alpha < 1$. In all cases, $\kappa = 2.5 \times 10^{-3}$ and $u_0 = 1$.

One can then identify three distinct regimes of gray soliton refraction, which are distinguished solely by the value of α. These are illustrated in Figs. 4(b), 4(c), and 4(d).

First, for linear step interfaces ($\alpha = 1$), one finds that $\theta_{0t} \simeq \theta_{0i}$. The predictions of Eq. (13) are plotted in Fig. 4(b) for different values of F in this regime. It is revealed that gray solitons propagating at significant angles refract in a manner that closely matches black soliton refraction. Second, for interfaces with a larger Kerr coefficient in the second medium ($\alpha > 1$), one obtains $\theta_{0t} > \theta_{0i}$. A larger value for θ_{0t} entails a reduction in the net angle of refraction θ_{nt}, as dictated by Eqs. (7) and (13). Such dependency is mapped out in Fig. 4(c) for the same values of F as in Fig. 4(b), and shows the trend of decreasing θ_{nt} with increasing F. Figure 4(c) also reveals a further feature that has not previously been reported (in accounts of either bright or black soliton refraction). It is found that a gray soliton may undergo either external or internal refraction, depending solely on the angle of incidence and provided that both interface and soliton grayness parameters are properly chosen. Finally, a different trend with respect to F variation is obtained in the third regime, where $\alpha < 1$. Predictions are shown in Fig. 4(d). Here, nonparaxial net angles of refraction are found to increase with increasing F, which is consistent with $\theta_{0t} < \theta_{0i}$, as shown in Fig. 4(a). In this case, angular corrections are not as large as those shown in Fig. 4(c) as a result of the $\alpha^{1/2}$ dependency of Eq. (15).

IV. LINEAR STEP INTERFACES

Theoretical predictions for the various parameter regimes have been tested against an extensive series of simulations involving full numerical integration of the NLH equation. Our account of this comparison starts with an analysis of linear step interfaces.

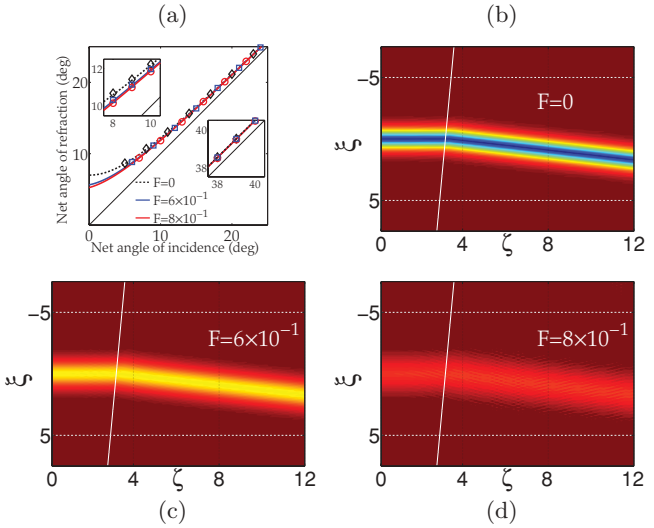

FIG. 5. (Color online) Dark soliton refraction for a linear step interface ($\alpha = 1$) with $\Delta = -0.015$ and $\kappa = 10^{-3}$. (a) Theory (curves) and numerical data (diamonds, squares, and circles). Simulation snapshots for the same interface considered in part (a), when $\theta_{ni} = 40^{\circ}$ and soliton grayness is (b) $F = 0$, (c) $F = 0.6$, and (d) $F = 0.8$.

Net angles of incidence θ_{ni} and refraction θ_{nt} are displayed in Fig. 5(a) for a linear step interface with $\Delta = -0.015$ and for three different values of soliton grayness. Lines are analytical predictions, while diamonds, squares, and circles represent results from numerical integration of the NLH equation for $F = 0$, $F = 0.6$, and $F = 0.8$, respectively. The agreement found between theory and numerics extends to all angles of incidence and values of F considered. The two insets of Fig. 5(a) highlight results for low (left) and moderate (right) angles of incidence. The predicted small differences (between black and gray soliton refraction) at low angles are verified, and these differences are confirmed to decrease as the angle of incidence grows, whereby all solitons undergo approximately the same angle of refraction. The detail in the right inset of Fig. 5(a) confirms this, showing diamonds, squares, and circles superimposed. Typical results from full simulations are shown in Figs. 5(b), 5(c), and 5(d). Here, soliton refractions for $F = 0$, $F = 0.6$, and $F = 0.8$, respectively, and a net incidence angle of $\theta_{ni} = 40^{\circ}$ are shown. Hence, solitons in this regime mostly undergo an angle of refraction that is independent of the precise value of F.

V. TOTAL NONREFRACTION ANGLE

Refraction properties of bright and black solitons at nonlinear interfaces are determined by an overall mismatch parameter involving both linear and nonlinear contributions [76]

$$\delta_{\pm} = \Delta + 4\kappa\beta_{\pm}(1 - \alpha). \tag{16}$$

For bright and black solitons, only the sign of $\delta_{\pm}$ distinguishes three different scenarios: external refraction ($\delta_{\pm} < 0$), internal refraction ($\delta_{\pm} > 0$), and total transparency ($\delta_{\pm} = 0$) [75,76].

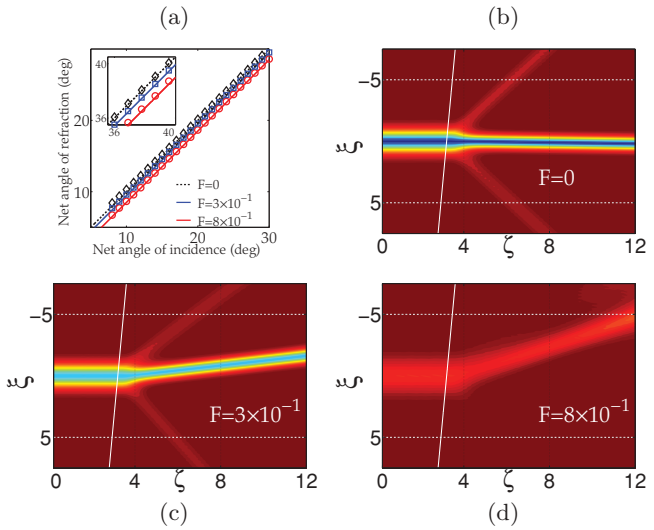

FIG. 6. (Color online) (a) Black and gray soliton refraction characteristics when the total transparency condition ($\delta_- = 0$) is met. Simulation snapshots for the same interface considered in part (a), when $\theta_{ni} = 40^o$ and soliton grayness is (b) $F = 0$, (c) $F = 0.3$, and (d) $F = 0.8$.

In the case of gray solitons, this criterion is no longer valid since intrinsic gray velocity components also affect net angles of incidence and refraction.

This feature is illustrated in Fig. 6(a), where interface parameters $\alpha = 3$ and $\Delta = -0.008$ have been chosen to provide total transparency for a black soliton. Here, $u_0 = 1$ and $\kappa = 10^{-3}$, thus giving $\delta_- = 0$ in Eq. (16). The dotted black straight line charts the refraction of black solitons according to Eq. (13). The blue (black) solid line displays gray soliton refraction for $F = 0.3$, while the case of $F = 0.8$ is represented by the red (gray) solid line. The results show that, for fixed F, gray solitons incident under the total transparency condition for the corresponding black solitons undergo the same angular deflection ($\theta_{nt} - \theta_{ni}$), regardless of the angle of incidence. The magnitude of this deflection depends on F, and can be either positive ($\alpha < 1$) or negative ($\alpha > 1$). Theoretical predictions show excellent agreement with results extracted from full numerical simulations. Diamonds, squares, and circles represent numerical data for $F = 0$, $F = 0.3$, and $F = 0.8$, respectively. The inset of Fig. 6(a) highlights such agreement when larger net angles of incidence are considered. For this interface, $\alpha > 1$ and the net angle of refraction is reduced for gray solitons; the extent of internal refraction becomes greater as F increases. This trend is mapped out in Figs. 6(b), 6(c), and 6(d), where refractions of black and gray solitons are illustrated for $\theta_{ni} = 40^o$.

To quantify gray soliton behavior, instead of the former total transparency condition, we define a total nonrefraction angle. A substantial difference is that, for example, total nonrefraction (if possible) can only be achieved for a single angle of incidence. This is shown in Fig. 7(a), where the refraction of a gray soliton with $F = 0.7$ is considered for two different nonlinear interfaces. The intersection of Snell's-law curves and the straight line $\theta_{ni} = \theta_{nt}$ provides the total nonrefraction angle in each case.

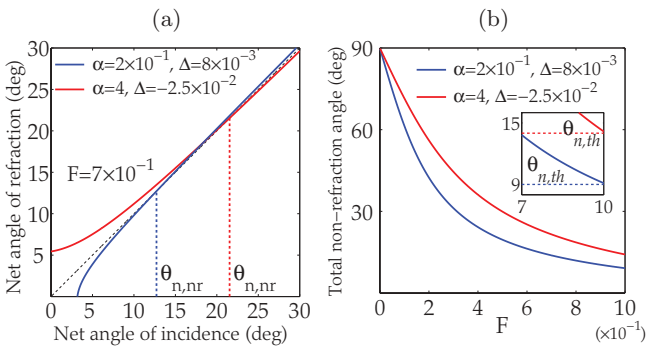

FIG. 7. (Color online) (a) Determination of total nonrefraction angles $\theta_{n,nr}$ for two nonlinear interfaces. (b) Nonrefraction angles as a function of F, for the same interfaces considered in part (a). $\kappa = 5 \times 10^{-4}$ in both figures.

An analytical expression for the total nonrefraction angle $\theta_{n,nr}$ is thus obtained when the condition $\theta_{ni} = \theta_{nt}$ is met in Eq. (13):

$$\gamma_- n_{01} \cos(\theta_{n,nr} + \theta_{0i}) = n_{02} \cos(\theta_{n,nr} + \theta_{0t}), \qquad (17)$$

which leads to

$$\tan(\theta_{n,nr}) = \frac{n_{01} n_{02}^{-1} \gamma_- \cos(\theta_{0i}) - \cos(\theta_{0t})}{n_{01} n_{02}^{-1} \gamma_- \sin(\theta_{0i}) - \sin(\theta_{0t})}. \qquad (18)$$

Figure 7(b) plots Eq. (18) as a function of F for the same two nonlinear interfaces considered in Fig. 7(a). As $F \to 0$, the gray soliton trajectories are seen to converge to those of the reference black soliton at normal incidence. Moreover, the inset of Fig. 7(b) also reveals that, for each nonlinear interface, there is a total threshold angle $\theta_{n,th}$ that presents a minimum angle of incidence necessary to obtain this phenomenon. Any paraxial analysis, with its validity restricted to vanishingly small angles of incidence, is thus not expected to accurately capture total nonrefraction behavior.

Numerical evidence of total nonrefraction is shown within the series of frames of Fig. 8. The behavior of a gray soliton with $F = 0.4$, impinging on a nonlinear interface with $\alpha = 2$ and $\Delta = -0.013$, is examined. These parameters give $\theta_{n,nr} = 30.35^o$. The predictions of Eq. (13) are plotted for three different ranges of angle of incidence: $\theta_{ni} < \theta_{n,nr}$; $\theta_{ni} \approx \theta_{n,nr}$; and $\theta_{ni} > \theta_{n,nr}$. The results are shown in Figs. 8(a), 8(b), and 8(c), where external refraction, total nonrefraction, and internal refraction are demonstrated, respectively (depending solely on the angle of incidence). In all cases, there is excellent agreement between numerical data (points) and analytical results (solid curves). In Fig. 8(b), both points and solid lines are superimposed upon the dashed line representing the $\theta_{ni} = \theta_{nt}$ condition. Individual simulations, illustrating external refraction, total nonrefraction, and internal refraction, are presented in Figs. 8(d), 8(e), and 8(f), respectively.

The total nonrefraction angle can play an analogous role to that of the critical angle in the context of bright solitons. Nonlinear interfaces have been proposed as switching elements, in which a bright soliton is either reflected or transmitted depending on the angle of incidence. For the case of gray solitons, nonlinear interfaces can also be proposed as a basis for designing further nonlinear devices. Operational

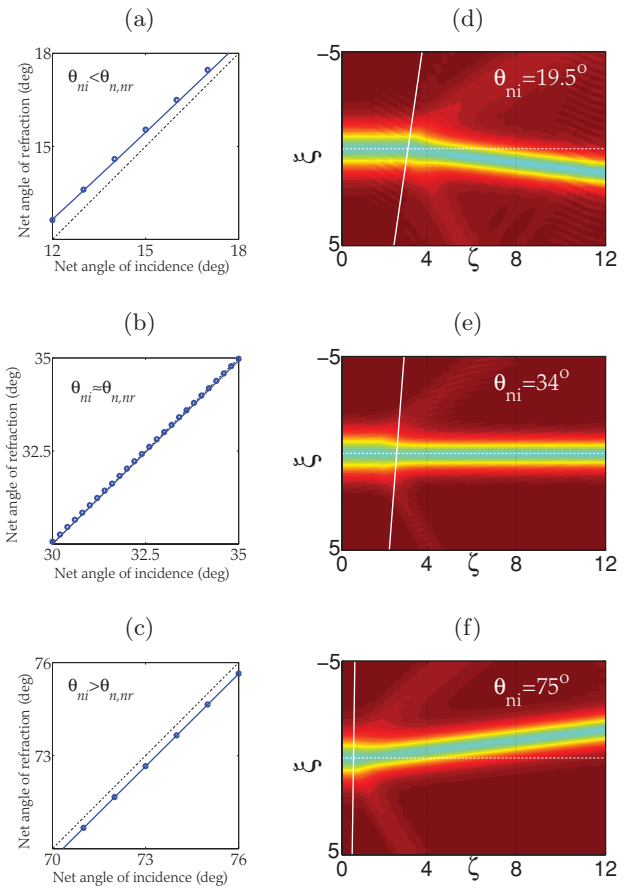

FIG. 8. (Color online) Gray soliton refraction for $F = 0.4, \alpha = 2$, $\Delta = -0.013$, and different ranges of net incidence angle. (a) external refraction, (b) total nonrefraction, and (c) internal refraction are obtained when $\theta_{ni} < \theta_{n,nr}$, $\theta_{ni} \approx \theta_{n,nr}$, and $\theta_{ni} > \theta_{n,nr}$, respectively. Simulation snapshots, corresponding to these three scenarios, are presented in (d), (e), and (f).

principles, in which an interface can act as either a focusing or a defocusing lens in the manipulation of arrays of soliton beams, are sketched in Fig. 9.

In Fig. 9(a), two arrows represent two gray solitons incident at different angles to the interface. One soliton has $\theta_{ni} < \theta_{n,nr}$, and thus undergoes external refraction, while the other soliton has $\theta_{ni} > \theta_{n,nr}$, and hence experiences internal refraction. The

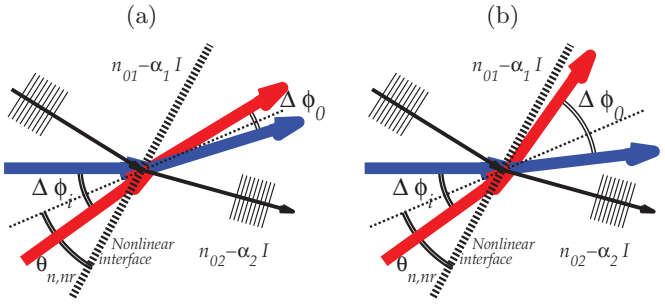

FIG. 9. (Color online) (a) Narrowing or focusing of soliton trajectory angle range in the vicinity of $\theta_{n,nr}$ for an $\alpha > 1$ and $\Delta < 0$ interface. (b) Broadening or divergence of the angular range of soliton paths around $\theta_{n,nr}$ for an $\alpha < 1$ and $\Delta > 0$ interface.

action of the interface is therefore quite similar to that of a converging (positive) lens, in which dark soliton trajectories play the role of optical rays. For this type of interface, an array of soliton beams that are diverging at an angle $\Delta\phi_i$ undergo angles of refraction that tend to $\theta_{n,nr}$, so that the angular spread of trajectories is reduced ($\Delta\phi_o < \Delta\phi_i$). The interface thus gathers soliton paths to within the proximity of $\theta_{n,nr}$. The possibility of complementary (i.e., dispersive) operation is sketched in Fig. 9(b). For example, this could correspond to the $\alpha = 0.2$ interface characterized in Fig. 7(a), for which external refraction occurs when $\theta_{ni} > \theta_{n,nr}$, and vice versa. In this case, the interface acts as the equivalent of a diverging (negative) lens, as it increases the divergence of the soliton paths ($\Delta\phi_o > \Delta\phi_i$).

VI. NUMERICAL CONSIDERATIONS

An extensive series of large-scale numerical simulations has played a fundamental role in this work, and has enabled a thorough investigation of analytical predictions. Simulations employed a nonparaxial beam propagation method [81], which has been crucial in the development and validation of Helmholtz soliton theory [68–71,74–76]. All of the numerical results presented have exploited the rotational symmetry that a Helmholtz framework allows [66]. Instead of propagating each soliton with a nonzero transverse velocity toward an interface at $\xi = 0$, the interface was itself rotated. This scheme, which was used for both black and gray soliton refraction studies, greatly reduced computational requirements in terms of the need to sample sufficiently (potentially, rapidly varying) transverse phase variations. Even with this computational efficiency introduced, each simulation still involved a relatively huge number of transverse points. Typically, $115\,200 = 2^9 \times 15^2$ sampling points were used, which facilitated parallel code implementation among 15 processor cores [82].

The requirement of a very broad background beam to support the evolving solitons dictated the need for such large resources. The beam shape used was a raised cosine: $h(\xi) = \cos^2[\pi/rL(|\xi| - L_1)]$, if $L_1 < |\xi| < L_2$; $h(\xi) = 1$, if $|\xi| \leqslant L_1$; and $h(\xi) = 0$, if $|\xi| \geqslant L_2$, where roll-off factor $r = 0.5$, grid length $L = 160$, $L_1 = (1 - r)L/4$, and $L_2 = (1 + r)L/4$. Incident and refracted solitons needed to evolve on a flat, but finite, central portion of this background. This was assured by avoiding any role of the progressive spreading and evolution of the edges of the background field profile. To minimize evolution of this supporting beam prior to soliton refraction, each simulation was initiated at a point such that the background field encountered the interface in the early stages.

VII. CONCLUSIONS

In this work, we have presented analyses of dark soliton refraction at planar boundaries that separate two defocusing Kerr media. The study has been performed in the framework of Helmholtz theory, which permits valid results for arbitrary angles of incidence. A key finding is a generalized Snell's law that describes not only bright and black soliton refraction, but also the complexities involved in the refraction of gray solitons. The matching of exact soliton solutions at each side of the interface also yields expressions for the transverse

velocities and component angles of soliton trajectories, along with the general result that soliton grayness is conserved during refraction. Particular attention has been paid to parameter regimes in which linear and nonlinear effects have comparable magnitude. This allowed identification of distinct scenarios and regimes of behavior, where either all beam and interface effects come into play or when particular effects become dominant (such as in predominantly linear step interfaces). This focus on the relative importance of contributing effects should allow results to be applied to wider parameter regimes that share the same balance, or domination, of particular effects. All of the main theoretical predictions for these regimes have been thoroughly tested through comparison with full numerical solutions.

The refraction of gray solitons has been found to differ from bright or black soliton refraction at a fundamental level, since both external and internal refraction can be obtained at a single nonlinear interface (depending solely on the angle of incidence). This result followed from our introduction of the total nonrefraction angle (a unique angle of incidence under which a dark soliton refracts without trajectory deviation). Analytical expressions for nonrefraction angles have been provided, and these show that nonlinear interfaces can accommodate such a phenomenon provided one works over a certain (nonparaxial) angular threshold. Nonrefraction characteristics also led to a proposal that different types of planar interfaces may be employed for converging or diverging lens operations on dark soliton arrays.

Work is currently underway to analyze nonlinear surface waves, soliton breakup, and the Goos-Hänchen shift for Kerr-focusing interfaces, and also to quantify various generalizations of Helmholtz-nonparaxial soliton refraction arising from considerations of different classes of nonlinear materials. However, an account of these extended considerations is deferred until future publications.

ACKNOWLEDGMENTS

This work was supported by the Spanish Ministerio de Educación y Ciencia and Fondo Europeo de Desarrollo Regional, Project No. TEC2007-67429-C02-01, and Junta de Castilla y León, Project No. VA001A08.

[1] A. E. Kaplan, JETP Lett. **24**, 114 (1976) [Pis'ma Zh. Eksp. Teor. Fiz. **24**, 132 (1976)].
[2] A. E. Kaplan, Sov. Phys. JETP **45**, 896 (1977) [Zh. Eksp. Teor. Fiz. **72**, 1710 (1977)].
[3] N. N. Rozanov, Opt. Spectrosc. **47**, 335 (1979) [Opt. Spektrosk. **47**, 606 (1979)].
[4] W. J. Tomlinson, Opt. Lett. **5**, 323 (1980).
[5] D. Marcuse, Appl. Opt. **19**, 3130 (1980).
[6] P. W. Smith, W. J. Tomlinson, P. J. Moloney, and J.-P. Hermann, IEEE J. Quantum Electron. **17**, 340 (1981).
[7] W. J. Tomlinson, J. P. Gordon, P. W. Smith, and A. E. Kaplan, Appl. Opt. **21**, 2041 (1982).
[8] P. Varatharajah, A. B. Aceves, J. V. Moloney, and E. M. Wright, J. Opt. Soc. Am. B **7**, 220 (1990).
[9] D. R. Andersen, Phys. Rev. A **37**, 189 (1988).
[10] A. B. Aceves, J. V. Moloney, and A. C. Newell, J. Opt. Soc. Am. B **5**, 559 (1988).
[11] A. B. Aceves, J. V. Moloney, and A. C. Newell, Opt. Lett. **13**, 1002 (1988).
[12] A. B. Aceves, J. V. Moloney, and A. C. Newell, Phys. Rev. A **39**, 1809 (1989).
[13] A. B. Aceves, J. V. Moloney, and A. C. Newell, Phys. Rev. A **39**, 1828 (1989).
[14] P. J. Bradley and C. De Angelis, Opt. Commun. **130**, 205 (1996).
[15] Y. V. Kartasov, F. Ye, V. A. Vysloukh, and L. Torner, Opt. Lett. **32**, 2260 (2007).
[16] C. K. R. T. Jones and J. V. Moloney, Phys. Lett. A **117**, 175 (1986).
[17] N. N. Akhmediev, V. I. Korneev, and Yu. V. Kuzmenko, Sov. Phys. JETP **61**, 62 (1985) [Zh. Eksp. Teor. Fiz. **88**, 107 (1985)].
[18] E. M. Wright, G. I. Stegeman, C. T. Seaton, J. V. Moloney, and A. D. Boardman, Phys. Rev. A **34**, 4442 (1986).
[19] Y. M. Aliev, A. D. Boardman, K. Xie, and A. A. Zharov, Phys. Rev. E **49**, 1624 (1994).
[20] F. Ye, Y. V. Kartashov, and L. Torner, Opt. Lett. **32**, 394 (2007).
[21] B. R. Horowitz and T. Tamir, J. Opt. Soc. Am. B **61**, 586 (1971).
[22] T. Tamir and H. L. Bertoni, J. Opt. Soc. Am. B **61**, 1397 (1971).
[23] O. Emile, T. Galstyan, A. Le Floch, and F. Bretenaker, Phys. Rev. Lett. **75**, 1511 (1995).
[24] N. N. Akhmediev, Sov. Phys. JETP **56**, 299 (1982) [Zh. Eksp. Teor. Fiz. **83**, 545 (1982)].
[25] G. I. Stegeman, C. T. Seaton, J. Chilwell, and S. D. Smith, Appl. Phys. Lett. **44**, 830 (1984).
[26] G. I. Stegeman, E. M. Wright, C. T. Seaton, J. V. Moloney, T.-P. Shen, A. A. Maradudin, and R. F. Wallis, IEEE J. Quantum Electron. **22**, 977 (1986).
[27] C. T. Seaton, J. D. Valera, R. L. Shoemaker, G. I. Stegeman, J. T. Chilwell, and S. D. Smith, IEEE J. Quantum Electron. **21**, 774 (1985).
[28] A. D. Boardman and P. Egan, IEEE J. Quantum Electron. **21**, 1701 (1985).
[29] D. Mihalache, M. Bertolotti, and C. Sibilia, Prog. Opt. **27**, 229 (1989).
[30] G. I. Stegeman and C. T. Seaton, J. Appl. Phys. **58**, R57 (1985).
[31] G. I. Stegeman, C. T. Seaton, C. N. Ironside, T. J. Cullen, and A. C. Walker, Appl. Phys. Lett. **50**, 1035 (1987).
[32] R. Cuykendall and K. Strobl, J. Opt. Soc. Am. B **6**, 877 (1989).
[33] A. D. Boardman, P. Bontemps, W. Ilecki, and A. A. Zharov, J. Mod. Opt. **47**, 1941 (2000).
[34] G. Cancellieri, F. Chiaraluce, E. Gambi, and P. Pierleoni, J. Opt. Soc. Am. B **12**, 1300 (1995).
[35] J. Scheuer and M. Orenstein, Opt. Lett. **24**, 1735 (1999).
[36] J. Scheuer and M. Orenstein, J. Opt. Soc. Am. B **22**, 1260 (2005).
[37] P. W. Smith, J.-P. Hermann, W. J. Tomlinson, and P. J. Moloney, Appl. Phys. Lett. **35**, 846 (1979).
[38] P. W. Smith and W. J. Tomlinson, IEEE J. Quantum Electron. **20**, 30 (1984).

[39] K. H. Strobl and R. Cuykendall, Phys. Rev. A **40**, 5143 (1989).
[40] E. Alvarado Méndez *et al.*, Opt. Commun. **193**, 267 (2001).
[41] L. Jankovic, H. Kim, G. I. Stegeman, S. Carrasco, L. Torner, and M. Katz, Opt. Lett. **28**, 2103 (2003).
[42] F. Baronio, C. De Angelis, P.-H. Pioger, V. Couderc, and A. Barthelemy, Opt. Lett. **29**, 986 (2004).
[43] M. Peccianti and G. Assanto, Opt. Lett. **26**, 1690 (2001).
[44] M. Peccianti, K. A. Brzdakiewicz, and G. Assanto, Opt. Lett. **27**, 1460 (2002).
[45] G. Assanto and M. Peccianti, IEEE J. Quantum Electron. **39**, 13 (2003).
[46] M. Peccianti, C. Conti, G. Assanto, A. D. Luca, and C. Umeton, Nature (London) **432**, 733 (2004).
[47] M. Peccianti, G. Assanto, A. Dyadyusha, and M. Kaczmarek, Nature Phys. **2**, 737 (2006).
[48] M. Peccianti, A. Dyadyusha, M. Kaczmarek, and G. Assanto, Phys. Rev. Lett. **98**, 113902 (2007).
[49] M. Peccianti, G. Assanto, A. Dyadyusha, and M. Kaczmarek, Opt. Lett. **32**, 271 (2007).
[50] M. Peccianti, A. Dyadyusha, M. Kaczmarek, and G. Assanto, Phys. Rev. Lett. **101**, 153902 (2008).
[51] A. Piccardi, U. Bortolozzo, S. Residori, and G. Assanto, Opt. Lett. **34**, 737 (2009).
[52] G. Assanto, B. D. Skuse, and N. F. Smyth, Phys. Rev. A **81**, 063811 (2010).
[53] S. R. Serak, N. V. Tabiryan, M. Peccianti, and G. Assanto, IEEE Photonic. Tech. L. **18**, 1287 (2006).
[54] A. Alberucci, A. Piccardi, U. Bortolozzo, S. Residore, and G. Assanto, Opt. Lett. **35**, 390 (2010).
[55] A. Piccardi, A. Alberucci, U. Bortolozzo, S. Residori, and G. Assanto, IEEE Photonics Technol. Lett. **22**, 694 (2010).
[56] Y. V. Izdebskaya, V. G. Shevdov, A. S. Desyatnikov, W. Krolikowski, and Y. S. Kivshar, Opt. Lett. **35**, 1692 (2010).
[57] P. Varatharajah, A. C. Newell, J. V. Moloney, and A. B. Aceves, Phys. Rev. A **42**, 1767 (1990).
[58] I. V. Shadrivov and A. A. Zharov, J. Opt. Soc. Am. B **19**, 596 (2002).
[59] I. V. Shadrivov and A. A. Zharov, Opt. Commun. **216**, 47 (2003).
[60] N. Akhmediev, A. Ankiewicz, and J. M. Soto-Crespo, Opt. Lett. **18**, 411 (1993).
[61] Yu. S. Kivshar, A. M. Kosevich, and O. A. Chubykalo, Phys. Rev. A **41**, 1677 (1990).
[62] G. Fibich, Phys. Rev. Lett. **76**, 4356 (1996).
[63] S. Chi and Q. Guo, Opt. Lett. **20**, 1598 (1995).
[64] B. Crosignani, P. Di Porto, and A. Yariv, Opt. Lett. **22**, 778 (1997).
[65] A. Ciattoni, P. Di Porto, B. Crosignani, and A. Yariv, J. Opt. Soc. Am. B **17**, 809 (2000).
[66] P. Chamorro-Posada, G. S. McDonald, and G. H. C. New, J. Mod. Opt. **45**, 1111 (1998).
[67] P. Chamorro-Posada, G. S. McDonald, and G. H. C. New, J. Mod. Opt. **47**, 1877 (2000).
[68] P. Chamorro-Posada and G. S. McDonald, Opt. Lett. **28**, 825 (2003).
[69] J. M. Christian, G. S. McDonald, and P. Chamorro-Posada, Phys. Rev. E **74**, 066612 (2006).
[70] J. M. Christian, G. S. McDonald, and P. Chamorro-Posada, J. Phys. A: Math. Theor. **40**, 1545 (2007).
[71] J. M. Christian, G. S. McDonald, and P. Chamorro-Posada, Phys. Rev. A **76**, 033833 (2007).
[72] J. M. Christian, G. S. McDonald, and P. Chamorro-Posada, J. Phys A: Math. Theor. **43**, 085212 (2010).
[73] P. Chamorro-Posada and G. S. McDonald, Phys. Rev. E **74**, 036609 (2006).
[74] J. Sánchez-Curto, P. Chamorro-Posada, and G. S. McDonald, Opt. Lett. **32**, 1126 (2007).
[75] J. Sánchez-Curto, P. Chamorro-Posada, and G. S. McDonald, J. Opt. A: Pure Appl. Opt. **11**, 054015 (2009).
[76] J. Sánchez-Curto, P. Chamorro-Posada, and G. S. McDonald, Opt. Lett. **35**, 1347 (2010).
[77] S. R. Skinner and D. R. Andersen, J. Opt. Soc. Am. B **8**, 759 (1991).
[78] Y. Chen, Phys. Rev. A **45**, 4974 (1992).
[79] Y. V. Kartashov, V. A. Vysloukh, and L. Torner, Opt. Express **14**, 12365 (2006).
[80] P. Chamorro-Posada, G. S. McDonald, and G. H. C. New, J. Opt. Soc. Am. B **19**, 1216 (2002).
[81] P. Chamorro-Posada, G. S. McDonald, and G. H. C. New, Opt. Commun. **192**, 1 (2001).
[82] J. Sánchez-Curto and P. Chamorro-Posada, Parallel Comput. **34**, 539 (2008).